USB FLOW CHARACTERISTICS RELATED TO

NOISE GENERATION

W. H. Brown and N. N. Reddy
Lockheed-Georgia Company

SUMMARY

The effects of nozzle and flap geometry on USB flow field characteristics related to noise generation were examined experimentally using static models of two sizes. Flow attachment and spreading characteristics were observed using flow visualization techniques. Velocity and turbulence profiles in the trailing edge wake were measured using hot-wire anemometry, and the effects of the geometric variables on peak velocity and turbulence intensity were determined. Then, it is shown that peak trailing edge velocity is a function of the ratio of flow length to modified hydraulic diameter.

INTRODUCTION

Design concepts such as blown flaps, which provide high lift by turning and spreading the engine exhaust, necessarily produce more noise than would an undeflected jet. It is the problem of the designer to establish an acceptable balance between the performance of the aircraft and its noise. In this area, USB offers an apparent advantage over other techniques because the engine placement above the wing inherently provides noise shielding between the engine and the ground.

Performance and noise are directly related to flow characteristics. Performance evaluation generally involves only the gross properties of the flow field, such as mean velocity and pressure distributions, whereas noise evaluation requires knowledge of more detailed properties of the flow field, such as turbulence properties. The experimental work presented in this paper is directed toward understanding the role of turbulent flows interacting with rigid surfaces (wing and flap) in noise generation and propagation. Even so, some of the flow data obtained are applicable to performance evaluations. Radiated sound measurements and the analysis of noise sources given in references 1 and 2 provided some guidelines as to which flow characteristics might be pertinent in the determination of the noise characteristics of USB configurations. The results of flow visualizations, mean velocity and turbulence profiles, and the space-time cross correlations of fluctuating velocities in the trailing edge wake are presented.

212
PAGE INTENTIONALLY BLANK

EXPERIMENTAL MODEL AND APPROACH

Model designs and test conditions were kept general as befits an exploratory program and were selected to cover the range from CTOL through STOL aircraft. Nozzle and installation variables include nozzle size, shape, chordwise location on the wing, inclination and height above the wing. Flap variables include radius of curvature, deflection, and total flow-path length. Scale effects are provided by two model sizes.

The small-scale static model is shown in figure 1. This model, of 51 cm span, provided 5.08, 7.62, and 10.16 cm flap radii each at 30°, 45° and 60° deflection with provisions for a common flow length. The nozzle can be located off the surface or on the surface at any of three chordwise positions and at any desired impingement angle. Nozzles are provided in two sizes to simulate the range of engine by-pass ratio appropriate to the CTOL and STOL operation and in several shapes. Six nozzle shapes were used - circular, rectangular nozzles of aspect ratios 2, 4, and 4, D-shaped, and elliptical. The holes shown along the surface in this figure were used for surface static pressure measurements and with probe microphones to obtain space-time correlations of the fluctuating surface pressures.

The large-scale static model is shown in figure 2. This model, of 74 cm span, is approximately 2½ times the linear scale of the small model (except in span). A constant ratio of flap-radius-of-curvature-to-nozzle-height is maintained between the two model sizes. The large model corresponds to the 7.62 cm radius small-scale configuration at 30° and 60° deflection angles with nozzles of aspect ratios 4 and 8. Circular nozzles were provided also.

Flow visualizations provide a useful point of departure by showing in a qualitative way the extent and intensity of the flow field. Photographs of surface oil flow show flow attachment and spreading characteristics. Schlieren, being sensitive to density gradients in the flow, shows attachment in another perspective in addition to showing turning shocks, the overall jet boundaries, and possible large-scale structure in the jet.

Previous studies have indicated that the major source of USB noise is located in the vicinity of the trailing edge. For that reason, mean velocity and turbulence profile measurements were concentrated there. Fairly extensive sets of wake velocity and turbulence intensity profiles were obtained using the small-scale static model and a single-channel linearized constant temperature anemometer. The hot-wire was positioned parallel to the trailing edge and moved normal to the upper surface of the flap. Centerline values received the most attention because they more nearly represent two-dimensional behavior (which is easier to handle analytically) and because the centerline flow is more firmly attached to the surface, thereby having steeper velocity gradients and higher turbulence levels generated near the surface.

Space-time correlations of fluctuating velocities were measured in the vicinity of the trailing edge. Correlations of each component of the fluctuating velocity would have provided a better understanding of the turbulence structure and its role in noise generation. However, component-by-component correlation was not feasible at the time because only two-channel anemometry capability was readily available and because the yawed-wire technique is too cumbersome. Therefore, useful correlation measurements were made using two linearized hot-wire channels with an on-line digital correlator.

RESULTS AND DISCUSSION

Flow Visualizations

Oil flow visualizations were used early in the investigation to determine which configurations had attached flow at the trailing edge. Typical visualizations of separated and attached flow are shown in figure 3. These oil flow photographs were made with the aspect ratio 2 nozzle touching the wing at the 20% chord location and the 5.08 cm radius 60° deflection flap. The flow at the trailing edge is seen to be separated at 0° impingement angle and attached at 10° and 20°.

For nozzles discharging at the surface, flow impingement angle clearly is an important variable relative to flow attachment. For nozzles located off the surface, the height of the nozzle above the wing is equally important. With the exception of the circular nozzle, attached flow was obtained from all nozzles at an impingement angle of 20°. The circular nozzle due to its narrow width (almost zero) at the wing surface and its high center of momentum required a 30° impingement angle to achieve attachment.

Some configurations which exhibit attached flow at the trailing edge have local separations over the curved flap section as evidenced by the bubble seen in the oil flow photograph for a 10° impingement angle. All nozzles except the aspect ratio 8 nozzle (the thinnest one) showed a tendency toward this kind of local separation. Nozzle location and nozzle height affect the tendency to form a separation bubble. Moving the nozzle aft from the 20% chord location toward the flap increases the tendency toward separation presumably by allowing less opportunity for flow spreading and for velocity decay before the high-curvature flap is encountered. Greater nozzle inclination angles tend to reduce or eliminate separation bubbles by promoting flow spreading.

Schlieren photographs taken in the spanwise direction more clearly show separation than do the oil flow photographs which suffer somewhat from the effects of inertia. Schlieren photographs provide a means for distinguishing between a weakly attached and a separated flow when the oil flow observations are inconclusive as often is the case when the oil streaks near the trailing

edge are approximately parallel and cover only a narrow span. The Schlieren visualizations in figure 4 cover the range from separated through attached flow with the aspect ratio 8 nozzle and the 7.62 cm radius 60° flap.

The oil flow photographs in figure 3 were used in an attempt to quantify flow spreading. A spreading parameter defined as the sum of the scrubbed widths measured at the nozzle exit, the start and end of curvature, and the trailing edge was evaluated for several configurations. The results, plotted in figure 5, show the strong influence of impingement angle, nozzle size, and nozzle location on flow spreading. The difference in scrubbed area between the 20% chord location and the 50% chord location actually is greater than that indicated on the figure because the spreading parameter ignores the area increase which results from increased flow path length.

Velocity and Turbulence Profiles

Mean velocity and turbulence intensity profiles for four different nozzles are shown in figures 6 and 7. These profiles were taken along the centerline behind a 5.08 cm radius 60° deflection flap. The nozzles were touching the wing at the forward (20% chord) location and were inclined 20° relative to the wing. The circular nozzle and the rectangular aspect ratio 4 and 8 nozzles are twice the area of the aspect ratio 2 rectangular nozzle — 20.26 sq cm as opposed to 10.13 sq cm. The aspect ratio 2 and 4 nozzles have a common nozzle height — 2.25 cm. The circular nozzle and aspect ratio 8 nozzles have heights of 5.08 cm and 1.58 cm, respectively. Several characteristics of USB flow can be seen in these profiles.

Consider the shapes of the mean velocity profiles in figure 6. The profiles for the AR2 and AR8 nozzles are broader than the other two profiles and have more rounded peaks than does the profile for the AR4 nozzle. The magnitudes of the peak velocities decrease in the order: circular, AR4, AR2, and AR8. The location (in nozzle heights) of the peak velocity moves away from the surface in the order: AR4, AR8, circular, and AR2. Thus, we see that the magnitudes and locations of the peak velocity do not vary systematically with nozzle size, height, or aspect ratio when these variables are taken individually.

The turbulence intensity profiles in figure 7 correspond to the previously discussed mean velocity profiles. These profiles, some with one peak and others with two peaks, are less similar in shape than the mean velocity profiles. The dip between the peaks is related to the extent of development of the flow mixing profile. A deep dip (as does a high peak velocity) indicates a region of flow relatively unaffected by mixing and by boundary layer growth. The rounded profiles for the AR2 and AR8 nozzles are characteristic of a more advanced state of turbulence profile development.

Effects of Geometric Variables on Peak Velocity

It is believed that practical considerations such as internal losses and structural compatibility ultimately will require nozzles of low aspect ratio, say less than four. This results in a jet-dimension-to-flow-path-length which is short in terms of flow field development. More importantly, the inner profile at the trailing edge is in the initial stage of transition from a boundary layer profile before the edge to a jet mixing profile some distance into the wake region. Therefore, similarity profiles are not expected. However, peak values of mean velocity should vary consistently with the major geometric and operational variables.

The peak velocity and the turbulence intensity value at the knee of the turbulence profile were examined at the trailing edge in the mid-span plane for attached flow cases. Knee turbulence is used because the peak value, particularly for longer flow lengths, often occurs far from the edge and far from the high shear area where the noise source is presumed to be. Figure 8 shows how peak velocity and knee turbulence vary with the nozzle installation variables. The measured values were found to be "well behaved" with respect to the chosen variables. Peak velocity decreases as impingement angle increases and increases as the nozzle is moved aft (toward the flap) along the wing while maintaining a constant flow length. The first tendency is believed to be the result of jet spreading which increases the effective length-to-diameter ratio of the jet flow. The reason for the increase in velocity with nozzle chordwise position is not clear, although it might be related to the partial development of the flow before the flap is reached.

The effects of flap variables on peak velocity are shown in figure 9. Peak velocity decreases with increasing flap deflection, flap radius, and flow length. Only the relatively small decrease with increasing flap radius is surprising. The intuitive thought prior to testing had been that, other things being equal, peak velocity would decrease with decreasing radius of curvature because of the higher radial acceleration of the flow, and its greater tendency to separate.

Jet velocity profiles are expected to be functions of a length-to-diameter ratio. In the case of non-circular jets, hydraulic diameter is used with free jets and nozzle height (or jet thickness) is used with wall jets. Length usually is measured from the nozzle exit along the jet axis. In USB configurations where the jet follows a curved surface, flow length along that surface from the nozzle to the trailing edge is an appropriate length variable. It was reasoned that pure hydraulic diameter was inappropriate because it failed to account for the reduction in mixing area caused by the presence of the surface. Ultimately a modified hydraulic diameter based on nozzle perimeter diminished by the nozzle width was successful with "well attached" flows from all the small-scale static tests and some of the large-scale tests. The results are seen in figure 10.

Correlation Measurements

A typical set of space-time cross correlations of fluctuating velocities is shown in figure 11. These correlation measurements are normalized to the maximum value of the auto-correlation for the upstream wire which was located 1.6 cm aft and 0.1 cm above the trailing edge. Both hot-wires were parallel to the trailing edge.

Two things can be learned from the peaks of the cross-correlation curves. The slope of separation distance plotted against delay time at which the corresponding correlation peaks occur is the convection velocity of the turbulent field. It represents the velocity at which the turbulent structure is convected past the measuring locations. The envelope of the peaks provides a measure of eddy lifetime. By following the peaks, the observer effectively is moving with the eddy. The eddies lose their identity or coherence by decay and by coalescence. The time required for the correlation coefficient to reach 1/e of its maximum is defined as the eddy lifetime. It is a measure of the length of time the turbulent structure maintains its spectral identity.

The cross correlations at zero time-delay provide a measure of the size and isotropy of the turbulent structure. The length scale for a typical eddy is defined as the area under the curve of the zero-time cross-correlation coefficients plotted against the corresponding separation distances. The length scale or eddy size is a measure of the distance over which the structure maintains an amount of coherence. These length scales are defined in all directions - lateral and transverse as well as longitudinal. The ratios of the scales are measures of the isotropy of the turbulence. A ratio of unity indicates isotropic turbulence; other ratios indicate deviance from isotropy. We have used the ratio of streamwise to spanwise eddy sizes as the scale of anisotropy of the turbulence.

The correlation measurements shown in figure 11 were made in the wake of the 7.62 cm radius 60° deflection flap with the ARS nozzle inclined 20° relative to the wing at the 20% chord location. The measurements were made with a nozzle pressure ratio of 1.1. The corresponding peak trailing edge velocity is 74 m/s. The following values were obtained from that figure and a corresponding set of spanwise correlation measurements:

Convection Velocity	=	0.90 Peak Trailing Edge Velocity
Streamwise Length Scale	=	0.84 cm
Spanwise Length Scale	=	0.37 cm
Scale of Anisotropy	=	2.3

The use of these quantities in noise prediction is described in reference 2.

CONCLUDING REMARKS

It has been shown that the flow fields of realistic USB configurations are "well behaved" at least in respect to those gross characteristics, such as peak velocity, which are important in noise generation. Trends of peak velocity and turbulence intensity levels with respect to installational and operational variables appear to be reasonable and therefore should be usable in analyses of noise generation and of performance trends. These peak velocity trends when combined with a modified hydraulic diameter yielded a reasonable collapse of the peak trailing edge velocity data over a wide range of variables including model scale; flap radius, deflection, and length; and nozzle size, shape, location, and impingement angle.

The variation of trailing edge turbulence structure with geometric variables may be established with a more sophisticated experimental program using either four channel hot-wire anemometry or the four channel laser velocimeter developed recently at Lockheed.

REFERENCES

1. Gibson, J. S.; and Searle, N.: Characteristics of USB Noise. Powered-Lift Aerodynamics and Acoustics, NASA SP-406, 1976. (Paper no. 15 of this compilation.)

2. Reddy, N. N.; and Tam, C. K. W.: Analytical Developments for Definition and Prediction of USB Noise. Powered-Lift Aerodynamics and Acoustics, NASA SP-406, 1976. (Paper no. 16 of this compilation.)
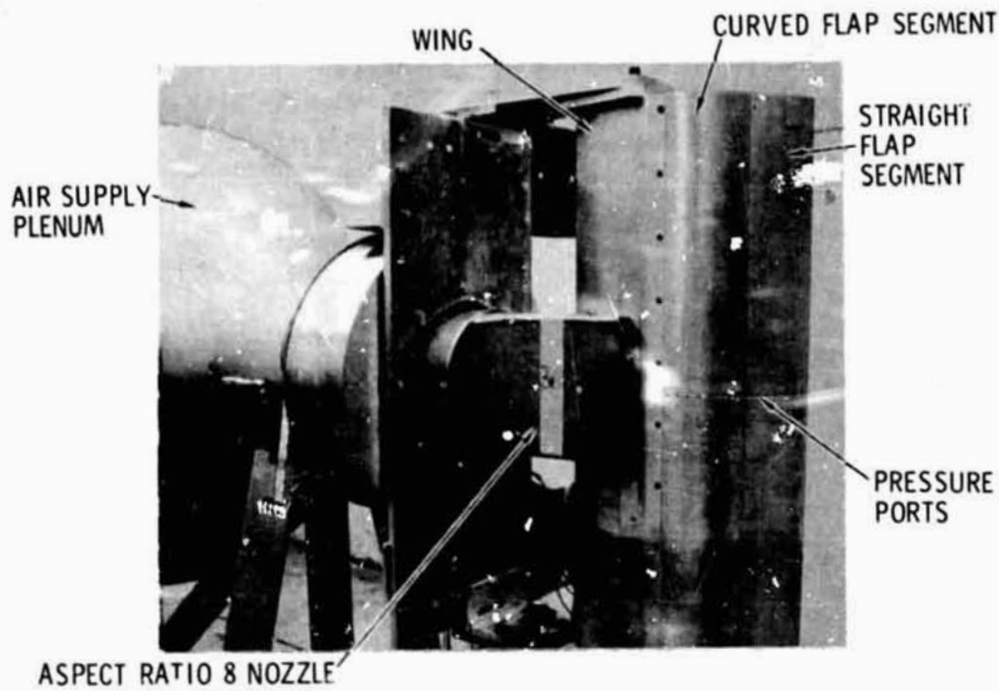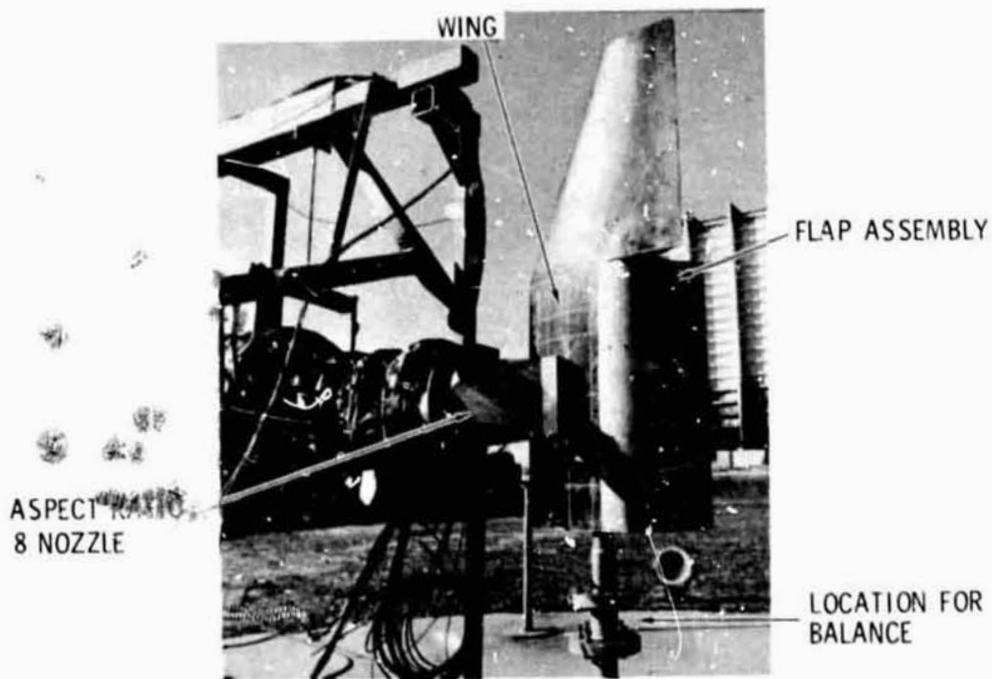
WING   CURVED FLAP SEGMENT

STRAIGHT
FLAP
SEGMENT

AIR SUPPLY
PLENUM

PRESSURE
PORTS

ASPECT RATIO 8 NOZZLE

Figure 1.- Small-scale test apparatus.

WING

FLAP ASSEMBLY

ASPECT RATIO
8 NOZZLE

LOCATION FOR
BALANCE

Figure 2.- Large-scale test apparatus.

0°   10°   20°

IMPINGEMENT ANGLE
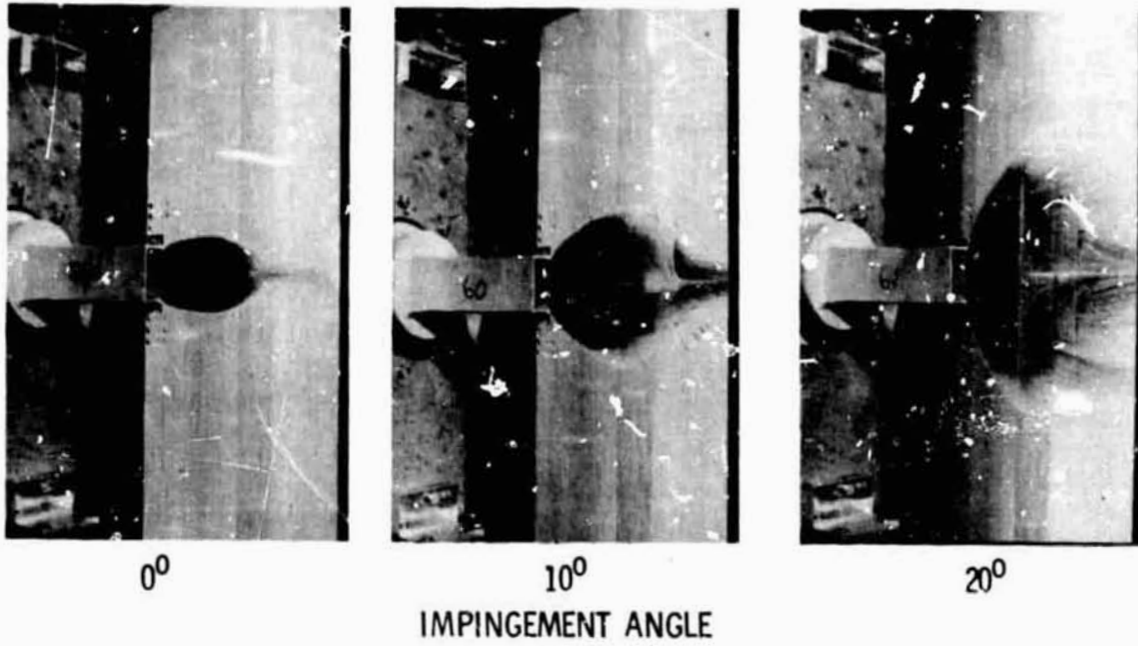
Figure 3.- Oil flow visualizations.

0°   10°   20°

IMPINGEMENT ANGLE
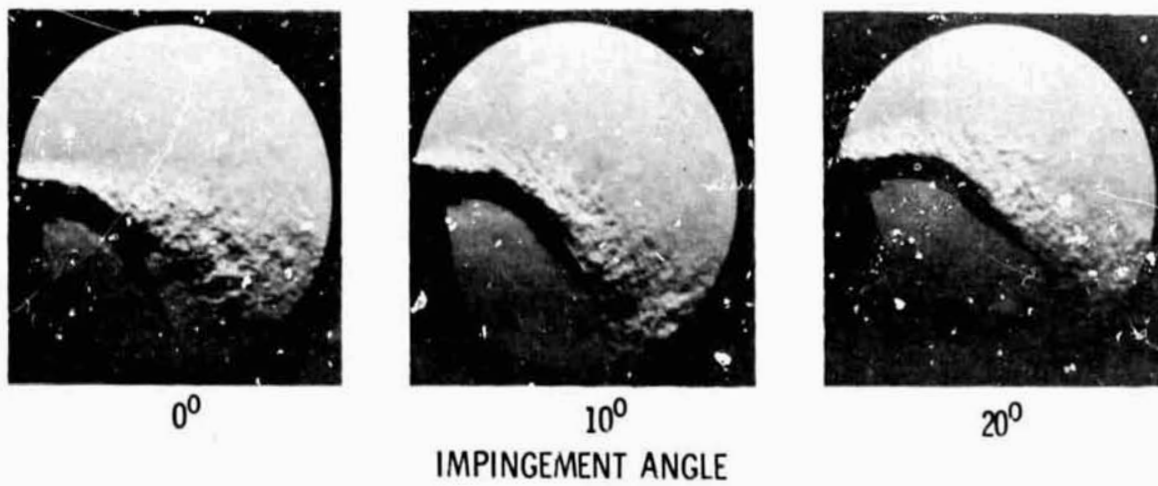
Figure 4.- Schlieren flow visualizations.
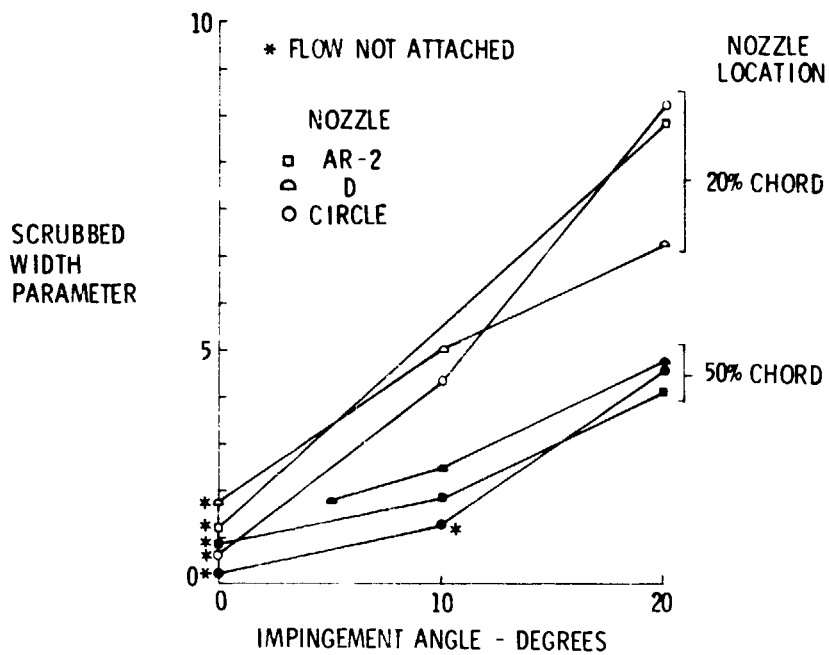
Figure 5.- Effect of nozzle variables on scrubbed width.
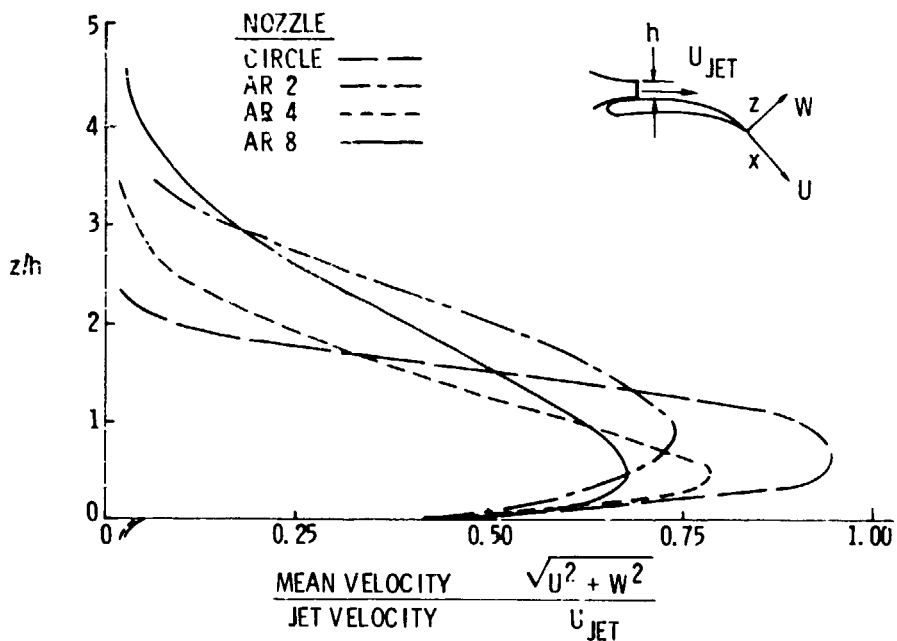
Figure 6.- Typical trailing edge mean velocity profiles.

223

$$\frac{\text{TURBULENCE INTENSITY}}{\text{JET VELOCITY}} \quad \frac{\sqrt{u^2 + w^2}}{U_{JET}}$$
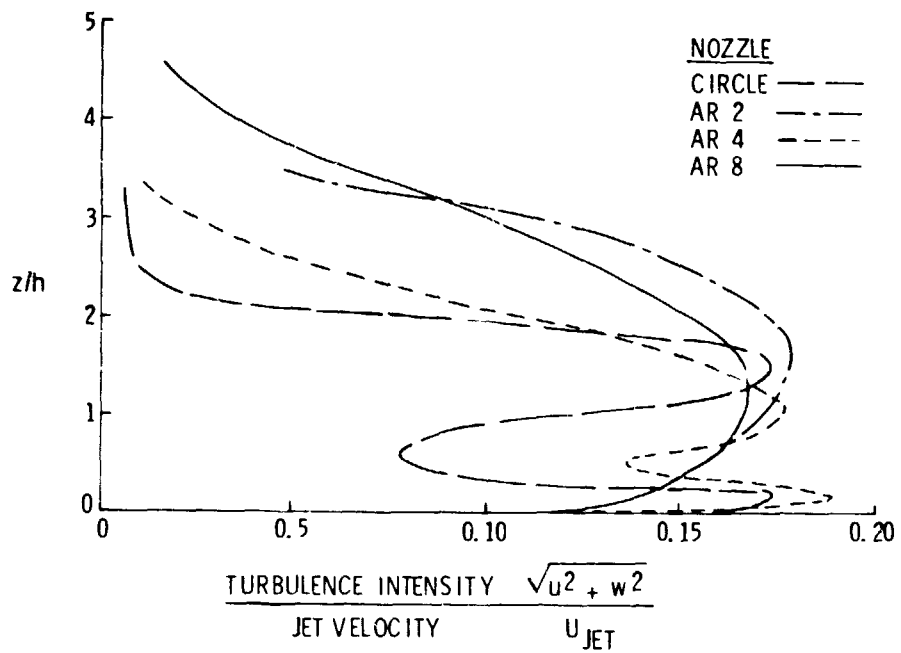
Figure 7.- Trailing edge turbulence profiles.
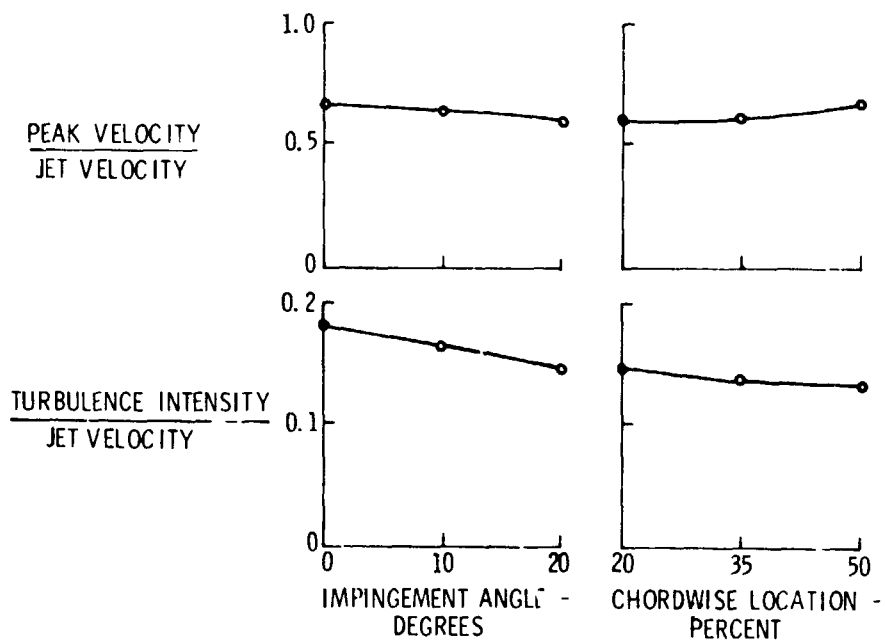
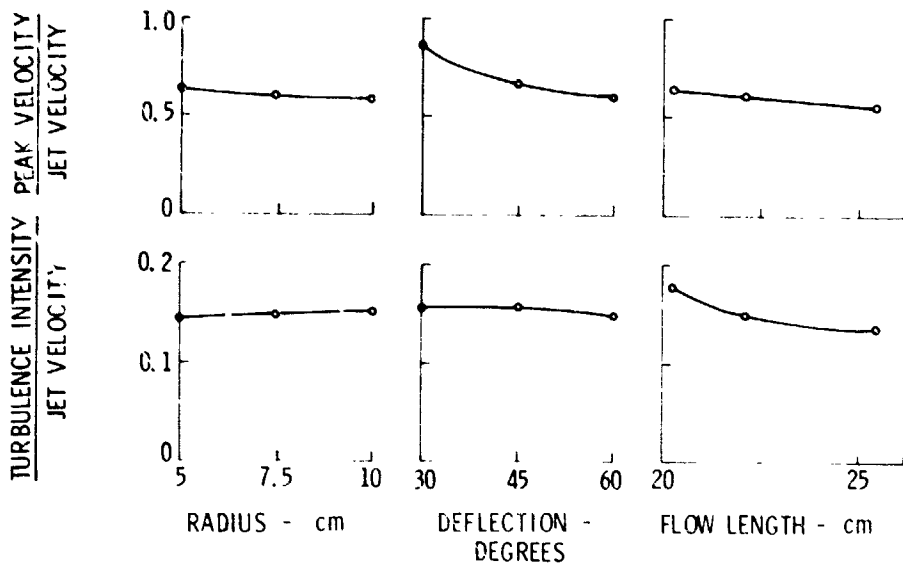
Figure 8.- Effect of nozzle installation variables.
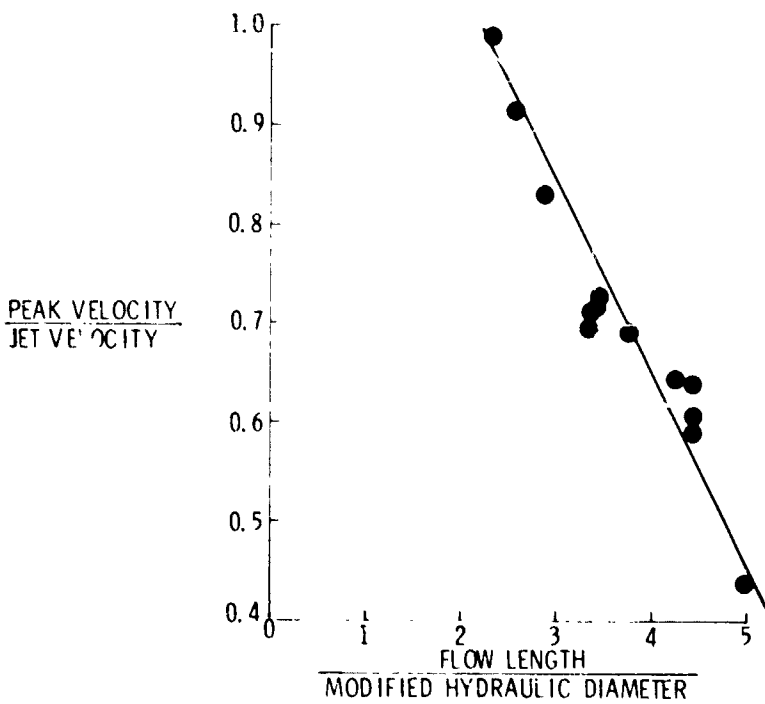
Figure 9.- Effect of flap variables and flow length.

Figure 10.- Effect of nozzle and flap geometry
on peak velocity.

SEPARATION
DISTANCE, $\bar{x}$, cm

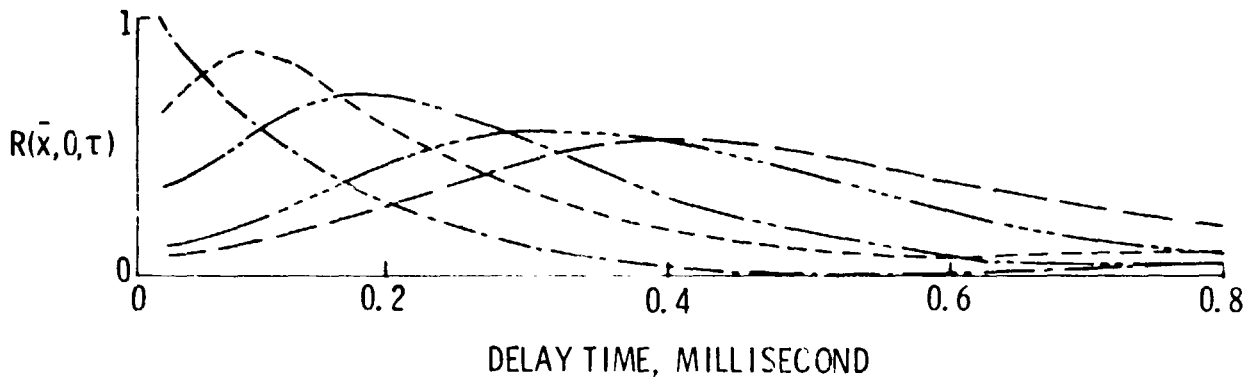| 0	— · —
.508	— — — —
1.016	— · —
1.78	— · · —
2.79	— — —

Figure 11.- Streamwise space-time fluctuating velocity
cross correlation